communications earth & environment

ARTICLE

https://doi.org/10.1038/s43247-021-00222-7 OPEN

Earth's core could be the largest terrestrial carbon reservoir

Suraj K. Bajgain [1✉], Mainak Mookherjee [1] & Rajdeep Dasgupta[2]

Evaluating carbon's candidacy as a light element in the Earth's core is critical to constrain the budget and planet-scale distribution of this life-essential element. Here we use first principles molecular dynamics simulations to estimate the density and compressional wave velocity of liquid iron-carbon alloys with ~4-9 wt.% carbon at 0-360 gigapascals and 4000-7000 kelvin. We find that for an iron-carbon binary system, ~1-4 wt.% carbon can explain seismological compressional wave velocities. However, this is incompatible with the ~5-7 wt.% carbon that we find is required to explain the core's density deficit. When we consider a ternary system including iron, carbon and another light element combined with additional constraints from iron meteorites and the density discontinuity at the inner-core boundary, we find that a carbon content of the outer core of 0.3-2.0 wt.%, is able to satisfy both properties. This could make the outer core the largest reservoir of terrestrial carbon.

[1] Earth Materials Laboratory, Earth, Ocean and Atmospheric Sciences, Florida State University, Tallahassee, FL, USA. [2] Department of Earth, Environmental and Planetary Sciences, Rice University, Houston, TX, USA. ✉email: sbajgain@fsu.edu

Earth's core is chiefly iron (Fe) but must contain some proportion of lighter elements to have the density based on the seismological observation[1–3]. However, the identity and proportion of the light elements are largely unknown[4–7]. Carbon is one of the important potential light-element candidates in the Earth's core because of its chemical affinity to the metallic phase and its cosmochemical abundance[4,8–10]. Carbon is highly soluble in metallic Fe-rich melt, with solubility reaching ≥5–8 wt.% at the core and core-forming magma ocean conditions[8,11,12]. Experiments that show such a high concentration of carbon in the Fe-rich melt are generally carbon saturated, whereas the carbon abundance in natural systems is expected to be well below the saturation limit imposed by graphite/diamond. To understand the behavior of carbon during large-scale melting during accretion and constrain its abundance in the mantle and core, the partition coefficient of carbon between Fe-rich alloy melt and silicate melt, $D_C^{metal/silicate}$ has been estimated over the past decade. The high-pressure–temperature laboratory experiments show that $D_C^{metal/silicate}$ is always >1, i.e., it behaves as a siderophile element under core-forming conditions[12–24].

Although all studies point toward the siderophile behavior of carbon, there remains a debate on the extent of its siderophile behavior. Most studies, especially for alloy compositions that are poor in other light elements such as S, Si, and N determined $D_C^{metal/silicate}$ values in the order of hundreds to thousands[13,15–18,20]. Whereas some studies argued for $D_C^{metal/silicate}$ values for systems containing S-poor Fe-rich alloy as low as ~5–50[23–25]. In a recent study, it is not only argued in favor of much lower $D_C^{metal/silicate}$ at very deep magma ocean conditions, combining lower pressure data, but a strong negative pressure dependence of $D_C^{metal/silicate}$ has also been reported[23]. Yet, based on experimental data to 15 GPa no such negative pressure effect has been observed. A weaker preference of C for Fe-rich metallic melt in the recent studies is at odds with the first-principles molecular dynamics (FPMD) simulation on the speciation of carbon in silicate melt with pyrolytic composition, which suggests that the significant amount of carbon can be partitioned into iron-rich metal based on the strong clustering between iron and carbon[26]. The uncertainty in the carbon budget of the Earth's outer core does not only stem from the uncertainty in the extent of siderophile behavior of C during magma ocean processes. It is also related to the poorly constrained concentration of carbon in inner Solar System planetary bodies during accretion as well as the extent of alloy-silicate equilibration during core formation. Because of these various sources of uncertainties, the estimated carbon content of the Earth's core based on models of accretion and alloy-silicate differentiation varies by about a factor of 30, i.e., from ~0.1 to ~3 wt.%[12,20,23,24,27].Therefore, an independent estimate of the carbon content of the Earth's present-day outer core, based on other approaches, is highly desirable.

The carbon budget of the Earth's outer core has also been estimated using the partitioning behavior of carbon between liquid iron and condensed phase of iron, i.e., hcp Fe, which indicates that carbon preferentially partitions into liquid outer core[28]. Based on this strong partitioning of carbon in the liquid outer core, it is predicted that 1.5–2 wt.% carbon in the outer core can explain the density discontinuity of 4.5–6.5% at the inner and outer core boundary (ICB) if carbon was the only light element[28–30]. However, the density deficit in the Earth's inner core cannot be explained if no other light elements are present in the inner core. High-pressure and temperature-phase diagram of Fe–C alloy has also been used to constrain the carbon content of the Earth's core. Previous phase relation experiments on Fe–C system have shown that either carbon dissolved in hcp Fe as an interstitial defect or Fe_7C_3 phase could crystallize at inner-core conditions[11,31–33]. Based on the eutectic temperature in Fe–C phase diagram, Earth's outer core could contain <3 wt.% C and the inner core could contain <1 wt.% C[33]. The carbon content estimated using the phase diagram can partially account for the shear wave velocity anomaly, anisotropy, and Poisson's ratio of the inner core[34–36]. Yet, 1 wt.% C cannot adequately compensate for the density deficit in the inner core. In addition, the presence of other light elements could limit the amount of carbon in the Earth's core[37]. Based on the melting temperature of pure Fe, ICB temperature varies from 5500 to 6300 K[38,39]. Light-element impurities could reduce the melting temperature of Fe at core pressures[40]. Thus, constraints on the concentration of light elements can also be deduced from the reduction of the melting temperature. Previous experiments suggest that reduction of melting temperature due to sulfur (S)[41], hydrogen (H)[42] could be as high as ~1000 K at ICB. In contrast, the effect of oxygen (O)[43] and silicon (Si)[44] of reduction of melting temperature are limited to 100 K. Carbon could reduce the melting temperature of iron by 600–800 K[40,45]. However, in a multi-component system with several light elements in the outer core, it is challenging to ascertain the reduction of melting temperature and provide constraints of the light-element concentration solely based on the core temperature.

Independent constraints on the carbon content of the Earth's core can be obtained by examining the effects of carbon on the density (ρ) and compressional wave velocity (V_P) of the iron alloy at pressure (P) and temperature (T) conditions relevant for the Earth's outer. Owing to the challenges associated with experiments at the conditions relevant for the Earth's outer core, the experiments constraining the ρ and V_P of Fe–C liquids are limited in pressure and temperature conditions (i.e., P < 10 GPa, T < 2500 K)[46–51]. Recently, in situ X-ray diffraction measurement have been performed at significantly higher P–T conditions of up to 58 GPa[52]. Similarly, the sound wave velocity of $Fe_{84}C_{16}$ liquid was measured using inelastic X-ray scattering up to 70 GPa[53]. Yet, large extrapolations are still required to estimate the ρ and V_P even at core–mantle boundary conditions, i.e., 136 GPa[52,53]. Since most of the experiments are performed at lower P–T conditions, an empirically established linear relationship between density and sound wave velocity, also known as Birch's law[54], is usually utilized to extrapolate density and elastic properties at core conditions[55]. However, the validity of Birch's law for solid iron at very high P–T is debated[56]. Thus, the first-principles molecular dynamics (FPMD) simulations can provide valuable insight into the density and elastic properties of metallic liquids at extreme P–T conditions relevant to Earth's core[57–62]. Recent FPMD simulation of liquid Fe–Ni–C at temperatures of ~1673 K and pressure ranging between 0 and 67 GPa demonstrated that the short-range liquid structure in FPMD simulation agrees well with the experiments at similar P–T conditions providing an essential benchmark for simulation[63,64].

Previous FPMD simulations were used to provide constraints on possible light-element candidates for the Earth's outer core considering Si, O, S, and C elements[6]. More recent FPMD studies examined the core composition and also included hydrogen as a potential light-element candidate at outer core compositions[65,66]. However, these studies were performed only at core P–T conditions with limited data points. Because of sparse data, reliable thermal equations of state for a particular alloy system are not available. In addition, the empirical correction used for adjusting pressure also varies among studies, and nitrogen as a light-element candidate was not considered in prior studies. Here, we explored Fe–C liquid binary systems with ~4, ~6, and ~9 wt.% of dissolved carbon at a wide range of pressure and temperature conditions i.e., 0–360 GPa and 4000–7000 K, covering those that are relevant for Earth's core. We also provide the thermal EOS and explore the validity of Birch's law. In order to validate our

Table 1 Density (ρ_0), bulk modulus (K_0), and the pressure derivatives of bulk modulus (K_0') for iron–carbon alloys at room pressure and various temperature (T) conditions.

Carbon (wt. %)	ρ_0 (gcm^{-3})	T (K)	K_0 (GPa)	K_0'	Method	Pressure conditions (GPa)	Temperature conditions (K)
3.83	4.86 ± 0.06	7000	27.2 ± 2.3	5.6 ± 0.1	FPMD	0–360	4000–7000[a]
6.01	4.62 ± 0.07	7000	23.6 ± 2.3	5.8 ± 0.1	FPMD	0–360	4000–7000[a]
8.91	4.37 ± 0.06	7000	21.5 ± 1.9	5.9 ± 0.1	FPMD	0–360	4000–7000[a]
5.68	7.23 ± 0.07	2273	124.6 ± 2.4	6.8 ± 1.1	FPMD	0–18	2273[b]
5.68	6.63 ± 0.04	2273	65.3 ± 12.8	8.4 ± 2.4	FPMD	0–18	2273[c]
3.50	6.91	1700	83.9	5.9 ± 0.2	XRA and US	0–4	1650–1850[d]
3.50	6.91	1700	55.3 ± 2.5	5.2 ± 1.5	XRA	2–7	1500–2200[e]
4.00	6.51	2500	110.0 ± 9.0	5.1 ± 0.3	IXS	7–70	1480–2700[f*]
6.70	6.50	1973	54.0 ± 3.0	4.0	XRA	3.6–9.5	1973[g]
2.85	6.00	3000	89.0	4.0	XRD	6–58	2000–3200[h]
2.85	6.00	3000	65.0	6.0	XRD	6–58	2000–3200[h]
4.00	6.82	1850	86.7 ± 1.6	6.0 ± 0.4	US	0–6	1700–2200[i*]
5.00	6.65	1673	70.1 ± 3.5	5.6 ± 0.3	FPMD	0–67	1673[j*]

FPMD first-principles molecular dynamics simulations, *XRA* X-ray absorption, *US* ultrasonic, *IXS* inelastic X-ray scattering, *XRD* X-ray diffraction experiment.
[a]BM3EOS fit parameter at 7000 K (this study). Pressure and density at other isotherms are obtained using Mie–Grüneisen thermal EOS (Eq. 1) $\left(\frac{dP}{dT}\right)_V = 26.2 - 42.1u + 17.2u^2$; $27.3 - 46.4u + 20.2u^2$; $28.3 - 51.3u + 23.8u^2$ for melt with ~4, ~6, and ~9 wt.% C, respectively.
$u = V/V_{ref}$ or ρ_{ref}/ρ ; $V_{ref} = 18.32$Å^3/atom (# atoms = 96); $\rho_{ref} = 4.44, 4.15, 3.82\,gcm^{-3}$ for melt with ~4, ~6, ~9 wt.% C, respectively; [b]BM3EOS fit parameter at 2273 K (this study); [c]BM3EOS fit parameter with correction of 8 GPa was added to the pressure calculated using FPMD
BM3EOS fit parameter from previous studies: [d]Shimoyama et al.[49]; [e]Shimoyama et al.[48]; [f]Nakajima et al.[53]; [g]Terasaki et al.[50]; [h]Morard et al.[52]; [i]Kuwabara et al.[51]; [j]Wang et al.[64]
[f*]Bulk modulus and the pressure derivative of bulk modulus are adiabatic. The isothermal bulk modulus (K_{0T}') is reported to be 82 GPa; [i*]properties are for Fe–Ni–C liquid with ~10 wt.% Ni and ~4 wt. % C; [j*]parameters are for Fe–Ni–C liquid with the composition $Fe_{3.7}Ni_{0.37}C$ (~5 wt. % C). Pressure correction of 7.2 GPa was added to the pressure calculated using FPMD.

simulation with high-pressure experiments[67,68], we use thermodynamically calculated pressure corrections. By combining the effects of C on Fe-liquid alloy density and compressional velocity with similar effects of the other five possible light elements (Si, N, O, S, and H) in the core, we directly constrain the possible carbon budget of the Earth's present-day outer core. We combine our outer core C content estimates with the bulk silicate Earth (BSE) C estimates from literature and provide new estimates for the bulk Earth (BE) carbon abundance.

Results

Our results show that the pressure (P), volume (V), and temperature (T) relationship of Fe–C binary melt can be represented using the Mie–Grüneisen thermal EOS

$$P(V,T) = P\left(V, T_{\mathrm{ref}}\right) + \left(\frac{\mathrm{d}P}{\mathrm{d}T}\right)_V \left(T - T_{\mathrm{ref}}\right) \quad (1)$$

where $P\left(V, T_{\mathrm{ref}}\right)$ is the pressure at reference isotherm and $\left(\frac{\mathrm{d}P}{\mathrm{d}T}\right)_V$ is the thermal pressure. We used 7000 K as our reference isotherm and the pressure–volume (density) relation along 7000 K can be described using the third-order Birch Murnaghan equation of state (Table 1). The thermal pressures $\left(\frac{\mathrm{d}P}{\mathrm{d}T}\right)_V$ are derived at constant volume or density using the linear relationship of pressure and temperatures along four isotherms, i.e., 4000–7000 K. Our result shows that the density of Fe–C liquid decreases with increasing carbon concentration along all isotherms (Fig. 1 and Supplementary Fig. S1).

To test the predicted pressures for a given density of a melt, we also simulated $Fe_{75}C_{21}$ (~5.7 wt.% carbon) at the constant temperature of 2273 K and compared with experimental melt density from X-ray absorption experiment[47]. We found that the predicted pressure from FPMD simulations is smaller than the experiments by ~8 GPa. So, we make an empirical positive pressure correction of 8 GPa to the calculated pressures. Corrected pressure-density data can be well described by a third-order Birch Murnaghan equation of state with $\rho_0 = 6.63 \pm 0.04\,gcm^{-3}$, $K_0 = 65.3 \pm 12.8$ GPa, $K_0' = 8.4 \pm 2.4$ (Table 1). Our zero pressure density (ρ_0) and the bulk modulus (K_0) are comparable with experimentally observed values from previous ultrasonic studies[48,50,51] and FPMD study of liquid Fe–Ni–C[64] (Table 1). In recent FPMD studies, the slight discrepancy between the pressure predicted from FPMD simulation and that of the experiments was addressed by adding constant empirical pressure correction to the FPMD results[6,57,60,64,69]. However, the recent computational study showed that the pressure difference between FPMD and experiment could vary both as a function of pressure and temperature[66]. Thus, a constant pressure correction for the entire core P–T conditions may not be sufficient. In our study, we have adopted a pressure correction constrained by thermodynamics ($P_{\mathrm{corr}}^{\mathrm{th}}$), which was implemented in previous FPMD studies[67,68] (Supplementary Note S1 and Supplementary Figs. S2–S4).

We estimate the Grüneisen parameter (γ) for carbon–iron alloys using the relation:

$$\gamma = \frac{V}{C_V}\left(\frac{\mathrm{d}P}{\mathrm{d}T}\right)_V \quad (2)$$

Our results indicate that the thermal Grüneisen parameter (γ) for iron–carbon alloy are ~1.0 at ambient pressure and increases upon further compression up to pressures of ~50 GPa. At higher pressures, γ uniformly decreases with increasing pressure (Supplementary Fig. S1). Thus, the value of γ continuously decreases from core–mantle boundary (CMB) to inner-core boundary (ICB). Comparison of γ for carbon-bearing metallic melt with that of pure iron form previous study shows that the carbon reduces the value of γ (Supplementary Fig. S1). The reduction of γ due to carbon is consistent with the effect of other light elements in previous studies of metallic melts, i.e., Fe–N and Fe–H liquids[59,61]. The pressure evolution of Fe–Fe coordination for all melt compositions shows an increase with increasing pressure up to ~50 GPa and beyond 50 GPa, Fe–Fe coordination remains mostly unaffected upon further compression (Supplementary Fig. S1). At high pressures, Fe–Fe coordination for pure iron is ~13, indicating the optimal packing Fe atoms similar to cubic closest packing (ccp) or hexagonal closest packing (hcp) of solid iron[59]. With increasing carbon concentration, Fe–Fe coordination decreases, from 12 to 10 for carbon concentration from 4 to 9 wt.% (Supplementary Fig. S1). The short-range atomistic scale structure of iron with 4 wt.% C also exhibits a nearly close-packed structure. However, the local network of iron atoms becomes less close-packed with increasing carbon concentration. The structural change manifests itself in the reduction of the density of

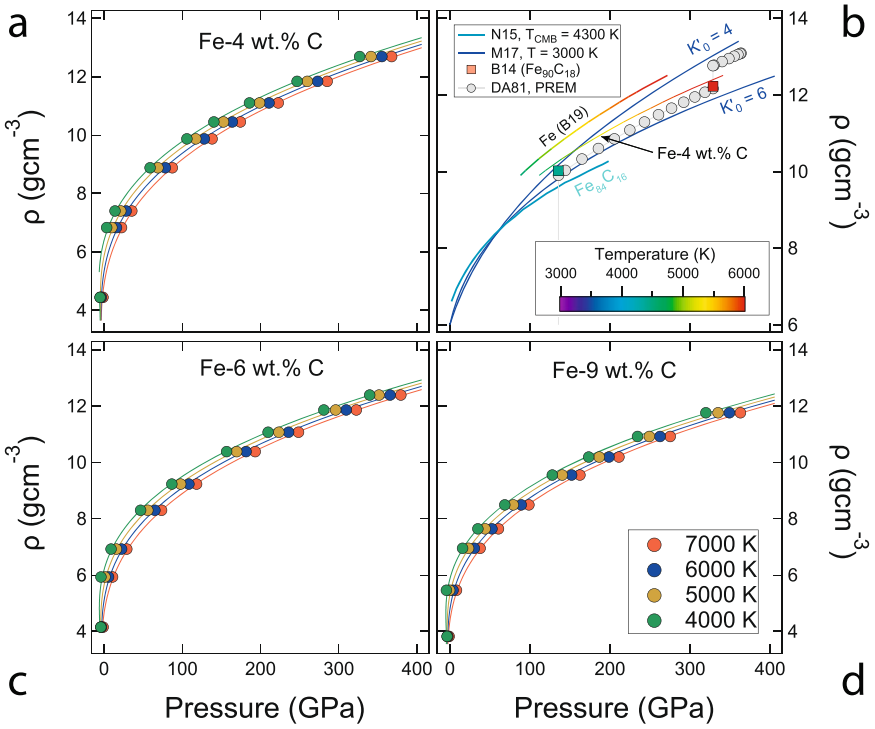

Fig. 1 Thermal equation of state of liquid Fe-C. Densities of iron alloy with (**a**, **b**) ~4 wt.%, (**c**) ~6 wt.%, and (**d**) ~9 wt.% of dissolved carbon as a function of pressure. Symbols are pressures estimated using first-principles molecular dynamics (FPMD) simulations at constant density, at 7000 K (red), 6000 K (blue), 5000 K (brown), and 4000 K (green). The pressure-density data from FPMD can be adequately described by a thermal equation of state (Table 1). Panel (**b**) shows the density of pure liquid iron, B19[59] and liquid Fe-4 wt.% C (this study) calculated along the geotherm with inner-core temperature (T_{ICB} = 6000 K) (Supplementary Fig. S2). Filled squares represent the density of liquid iron alloy with a stoichiometry of $Fe_{90}C_{18}$ (~4 wt.% C) from FPMD simulations at core conditions[6]. Experimental results of the density of liquid iron alloy with a stoichiometry of $Fe_{84}C_{16}$ (~4 wt.% C) liquid up to 200 GPa along geotherm (with T_{CMB} = 4300 K) is also shown (cyan line) for comparison[53]. Blues lines are the BM3 isothermal equation of state representation of liquid iron with ~3 wt.% carbon with $\rho_0 = 6.0\,gcm^{-3}$, $K_T = 89.0$ GPa, $K'_T = 4.0$, and $\rho_0 = 6.0\,gcm^{-3}$, $K_T = 65.0$ GPa, $K'_T = 6.0$[52]. Error in pressures represents ±1σ uncertainties which are smaller than the size of the symbols.

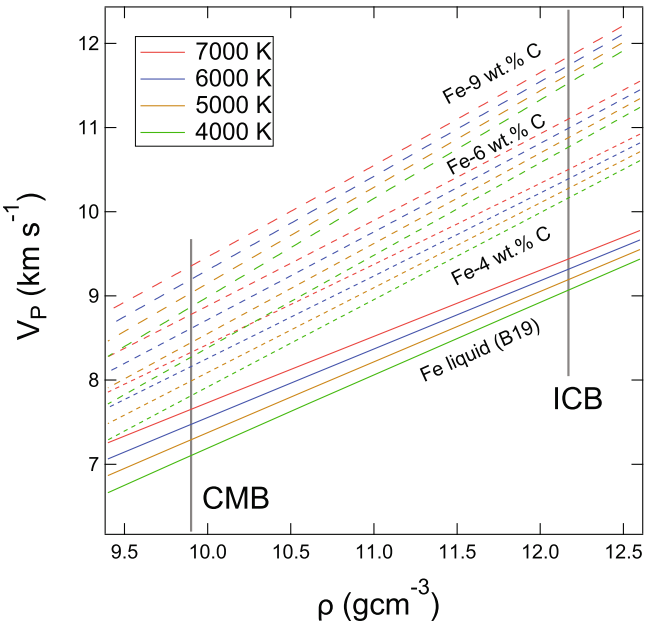

Fig. 2 Sound wave velocity of liquid Fe-C. Plot of calculated compressional wave velocity (V_P) for liquid Fe-C as a function of density (ρ) for various carbon concentrations, i.e., ~4, ~6, and ~9 wt.% along each isotherm: 7000 K (red), 6000 K (blue), 5000 K (brown), and 4000 K (green). Similar results for pure liquid Fe are from a previous FPMD study[59].

iron–carbon melts compared to that of the volatile free molten iron (Supplementary Fig. S1). P-wave velocity (V_P) of liquid iron–carbon can be calculated from

$$V_P = \sqrt{\frac{K_S + \frac{4}{3}G}{\rho}} \quad (3)$$

where K_S is the adiabatic bulk modulus, ρ is the density, G is the shear modulus. For the liquids where the frequency of the seismic probe is much smaller than the characteristic frequency of shear relaxation, shear modulus $G \to 0$[70]. The adiabatic bulk modulus (K_s) is related to the isothermal bulk modulus (K_T) by

$$K_s = K_T + \gamma T\left(\frac{dP}{dT}\right)_V \quad (4)$$

and,

$$K_T = -V\left(\frac{dP}{dV}\right)_T \quad (5)$$

Using both the γ and $\left(\frac{dP}{dT}\right)_V$ from FPMD simulations, we estimate the V_P for iron–carbon liquids at core conditions. Our result shows that the light-element carbon increases the V_P of liquid by ~94 ms^{-1} for each wt.% of dissolved carbon at core conditions (Figs. 2 and 3).

We estimate the ρ and V_P of Fe–C alloys at core conditions along the outer core geotherm. We assume that the temperature gradient in the outer core is adiabatic, the outer core temperature

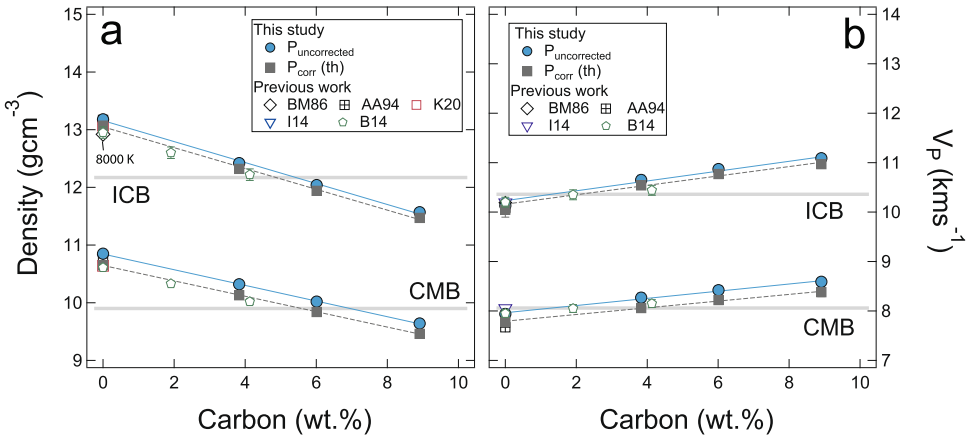

Fig. 3 Effect of carbon on the density (ρ) and compressional wave velocity (V_P) of liquid iron. Change in (**a**) ρ and (**b**) V_P of liquid Fe as a function of carbon content at core–mantle boundary (CMB: 136 GPa, 4400 K) and inner-core boundary (ICB: 330 GPa, 6000 K) conditions. Results for the metallic melts are from previous experimental studies, AA94, BM86, K20[106–108] and FPMD studies, B14, I14[6,58]. Lines show the linear relationship of ρ and V_P with the increasing amount of carbon (in wt.%). Filled gray squares represent the results after applying the thermodynamic pressure correction (P^{th}_{corr}) (Supplementary Note S1). When the pressure is adjusted using P^{th}_{corr}, the wt.% of carbon required to satisfy the seismic ρ and V_P becomes lower and higher, respectively. Error bars represent ±1σ uncertainties.

profile could be estimated from

$$\gamma(\rho) = \frac{\partial(\log T)}{\partial(\log \rho)} \quad (6)$$

Integrating Eq. (4) and assuming a fixed temperature (T_{ICB}) at the inner-core boundary (ICB) and adopting the density at ICB (ρ_{ICB}) from the preliminary reference Earth model (PREM) model, we derive an adiabatic temperature profile for the Earth's outer core[71]. Temperatures at ICB conditions are estimated to vary between 5500 and 6300 K based on the melting temperature of iron[38,39,72]. If the ICB temperature is held constant at 6000 K, based on the above approximation, the temperature at the core–mantle boundary (CMB) along the core adiabat is found to be ~4400 K. Similarly, if the ICB temperature is held at lower temperatures of 5400 and 5000 K, temperature at the core–mantle boundary (CMB) along the core adiabat are found to be ~4000 and ~3700 K, respectively (Supplementary Fig. S5). Our estimated outer core adiabat is in good agreement with the previous estimation based on thermodynamic parameters[57,59]. The temperature at the ICB will likely be lower if light elements are present. Previous work on Fe–C alloy estimated the melting temperature of Fe–C to be 5500 ± 500 K by considering the melting point depression of ~600–800 K[40,45].

For condensed matter phases such as solid minerals and alloys, the sound velocity often increases linearly with the density and is often referred to as Birch's law[54]. Birch's law is often used to extrapolate the elastic properties of the material from the low-pressure conditions to the core pressures. We tested the validity of Birch's law by comparing the bulk sound velocities of liquid iron and iron–carbon liquid along isotherms. Our results show that the isobaric temperature dependence of V_P for metallic melt, i.e., $\left(\frac{dV_P}{dT}\right)_P$ is negligible. However, V_P varies as a function of temperature at a constant density, i.e., V_P increases with increasing temperature at a fixed density (Fig. 2 and Supplementary Fig. S5). Our observations are similar to previous FPMD simulations on Fe-bearing metallic liquids, which found similar $\left(\frac{dV_P}{dT}\right)_P$ for liquid Fe, Fe–S, Fe–N, and Fe–H liquid[57,59,61,73]. This observation indicates that Birch's law may not hold for pure liquid iron as well as other metallic liquids such as Fe–C, Fe–S, Fe–N, and Fe–H at core pressure and temperature conditions. Our result also agrees with the previous experiment on solid iron that indicated a nonlinear relationship between density and sound wave velocity for hexagonal closed packed iron up to 73 GPa and 1700 K[56]. However, other studies on solid and liquid metals do not agree with ref. [56]. For example, density and sound wave velocity measurement for solid Fe up to 93 GPa and 1100 K shows that the density and sound wave velocity data do follow Birch's law[74]. Also, the shock-wave experiment of liquid Fe and liquid Fe–O–S do support Birch's law at much higher pressure up to 800 GPa[75,76].

Discussion

Our calculations allow us to estimate the ρ and V_P of liquid Fe–C at core pressure conditions along the adiabatic geothermal gradient. The adiabatic geothermal gradient was estimated by using a reference ICB temperature at 6000 K. Because the exact ICB temperature is unknown and there is a range of estimates, to account for any differences caused by the ICB reference temperature, we also evaluated the melt properties with reference ICB temperature at 5400 and 5000 K. To predict the carbon content of the Earth's outer core, we compare the ρ and V_P of iron–carbon liquid with the preliminary reference Earth model (PREM) values at CMB and ICB conditions[71]. We find a linear relationship for both ρ and V_P of Fe–C liquid alloy and the carbon content (X = wt.% of carbon), with $\left(\frac{d\rho}{dX}\right)_C < 0$ and $\left(\frac{dV_P}{dX}\right)_C > 0$ (Fig. 3).

For the core adiabat with $T_{ICB} = 6000$ K, we find that PREM density at core–mantle boundary (i.e., $T_{CMB} = 4400$ K) could be explained by 6.9 ± 0.4 wt.% of carbon dissolved in liquid iron alloy (Fig. 3). However, the estimated V_P for this amount of carbon exceeds seismological V_P at CMB. Our estimates on the carbon content of liquid iron alloy at CMB with $T_{CMB} = 4400$ K by matching V_P is ~1.3 ± 0.3 wt.% (Fig. 3). Similarly, at the inner-core outer core (ICB) boundary with $T_{ICB} = 6000$ K, we estimate the carbon content of 5.4 ± 0.2 wt.% and 1.3 ± 0.2 wt.%, by, respectively, matching ρ and V_P of Fe–C liquid alloy and PREM (Fig. 3). If we consider lower core temperatures, i.e., along adiabatic geothermal gradient with $T_{ICB} = 5400$ K, ~7.5 and ~5.8 wt.% carbon is necessary to explain ρ at CMB ($T_{CMB} = 4000$ K) and ICB ($T_{ICB} = 5400$ K) conditions, respectively (Supplementary Table S1). Similarly, for the temperature profile with $T_{ICB} = 5000$ K, a higher carbon amount, i.e., ~7.9 and ~6.1 wt.% is necessary to explain ρ at CMB ($T_{CMB} = 3700$ K) and ICB ($T_{ICB} = 5400$ K). We find that the wt.% of carbon is less sensitive to the core

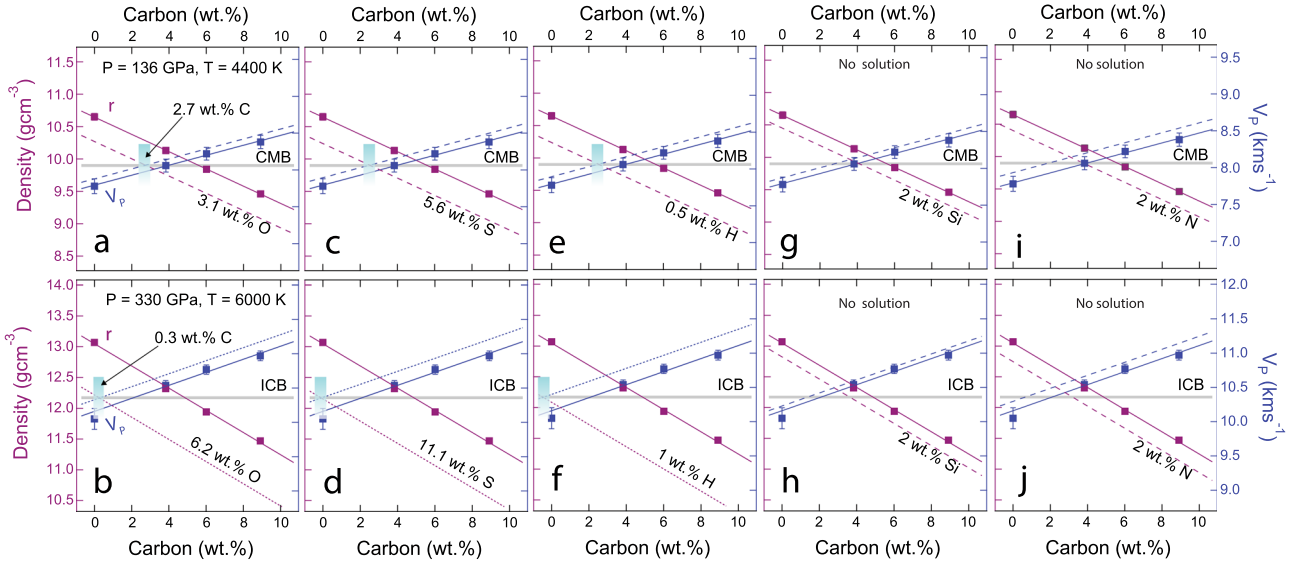

Fig. 4 Carbon content of the Earth's outer core. The effects of other light elements (**a**, **b**) oxygen, (**c**, **d**) sulfur, (**e**, **f**) hydrogen, (**g**, **h**) silicon, and (**i**, **j**) nitrogen at CMB (upper panels) and ICB conditions (lower panels) on the ρ and V_P of liquid iron as a function of carbon content. ρ is plotted on the left axes (purple) and V_P on the right axes (blue) in all panels. Pressure is corrected using thermodynamic constraints, P^{th}_{corr} (Supplementary Note S1). Thick gray line in each panel shows the density and compressional wave velocity at core conditions from preliminary reference earth model[71]. We note that the $\frac{d\rho}{dX_{LE}}$ and $\frac{dV_P}{dX_{LE}}$ for Si and N are very similar to that of carbon and hence it difficult to obtain a unique solution with Fe-Si-C and Fe-N-C ternary systems. Green bar in panels (**a**–**f**) indicates the unique solution in Fe-C-LE ternary that simultaneously explain ρ and V_P at ICB or CMB conditions. No unique solution is found for (**g**, **h**) Fe-C-Si and (**i**, **j**) Fe-C-N ternary systems. Error bars represent ±1σ uncertainties.

temperatures. For instance, the estimated wt.% of carbon required for explaining V_P at lower temperatures, i.e., $T_{ICB} = 5400–5000$ K and $T_{CMB} = 4000–3700$ K are same as that estimated for higher temperatures of $T_{ICB} = 6000$ K and $T_{CMB} = 4400$ K. This is due to the fact that at constant pressures and in the explored temperature range relevant for the Earth's outer core, i.e., between 3700 and 7000 K, the $\frac{dV_P}{dT}$ is negligible (Supplementary Fig. S5).

Effect of pressure correction is such that the estimated carbon content to match the seismic density decreases and the carbon content needed to match the velocity increases (Supplementary Note S1 and Fig. 3). For the geotherm with $T_{ICB} =$ 6000 K and pressure corrected using thermodynamic constraints (P^{th}_{corr}), Fe with ~4.9 wt.% carbon will satisfy PREM density at ICB condition, whereas liquid iron with ~5.6 wt.% carbon can reproduce PREM density at CMB pressure and 4400 K (Supplementary Table S1). However, Fe with ~2.1 wt.% and ~3.9 wt.% carbon is required to match the V_P at ICB and CMB conditions, respectively.

Our results at conditions relevant to the Earth's outer core indicate that Fe–C binary liquid alloy cannot simultaneously satisfy the ρ and V_P of the outer core. High-pressure studies based on in situ inelastic X-ray scattering suggested a 2.9–3.8 wt.% of carbon could explain the density deficit of the core[53]. However, 2.9–3.8 wt.% of carbon would translate to a V_P that is greater than the observed core V_P. In fact, a lower concentration of carbon, i.e., ~0.9–1.2 wt.% was required based on the comparison between V_P of the Fe–C alloy and the Earth's outer core[53]. More recently, in situ X-ray diffraction studies using a Paris–Edinburgh press and laser-heated diamond anvil cell of Fe–C liquid suggested that Fe with 1.8–3.7 wt.% carbon was sufficient to satisfy density profile at the core conditions[52]. Our results are in good agreement with an earlier FPMD simulations on Fe–C binary, which also found that Fe–C binary liquid alloy cannot simultaneously satisfy the ρ and V_P of the outer core, and around ~5 wt.% and ~2 wt.% of carbon is required satisfy core ρ and V_P, respectively[6] (Fig. 3). However, the actual carbon concentration in the core is expected to be lower than these estimates based on the study of Fe–C binary alloy due to the presence of other light elements.

Using the ratio of major and trace elements and assuming low-pressure core accretion under reducing conditions, it is estimated that the Earth's core may contain 7.35 wt.% Si, 2.30 wt.% S, and 4.10 wt.% O[5]. More recent core-formation models proposed that the Earth's core may contain 2 wt.% Si for a relatively oxidizing conditions[77] and 8–9 wt.% Si for reducing conditions[78]. Previous FPMD work indicated that 1.9 wt.% Si together with 3.7 wt.% O is the best match for both ρ and V_P of outer core[6]. In follow-up work, it was argued that an outer core composition that contains 2.7–5 wt.% oxygen and 2–3.6 wt.% silicon can also satisfy the geochemical constraints of core formation, i.e., such core-formation scenario can also result in a mantle with the observed abundance of key siderophile elements, such as Ni, Co, V, and Cr. Based on partition coefficients, sulfur-rich core with 8–10 wt.% S is suggested[79,80]. However, geophysical constraints indicate sulfur poor core with 2–3 wt.% S[81]. It was also concluded that the maximum sulfur in the Earth's outer core is <2.4 wt.% and it might be necessary to have oxygen in all the proposed compositional models for the outer core[6]. Shock-wave experiments on Fe–Si–O liquid indicated that the Earth's outer core may be oxygen poor with less than 2.5 wt.% O[76]. More recent FPMD work of Fe–S binary alloy set the upper limit of sulfur to 3.5 wt.%[62].

Since, the Earth's core likely contains other light elements such as oxygen, sulfur, silicon, hydrogen, and nitrogen in addition to carbon, we refine our estimates of the carbon content in the Earth's outer core based on the possibility of simultaneously explaining the ρ and V_P of core by considering a ternary mixture of Fe–C–LE where C, and LE refers to carbon and the other light elements, respectively–

$$\Delta\rho = \left(\frac{d\rho}{dX_C}\right)X_C + \left(\frac{d\rho}{dX_{LE}}\right)X_{LE} \quad (7)$$

$$\Delta V_P = \left(\frac{\mathrm{d}V_P}{\mathrm{d}X_\mathrm{C}}\right)X_\mathrm{C} + \left(\frac{dV_P}{\mathrm{d}X_\mathrm{LE}}\right)X_\mathrm{LE} \quad (8)$$

where, X_C and X_LE are weight fraction of carbon (C) and other light elements (LE); $\Delta\rho$ refers to $\left(\rho^\mathrm{Core} - \rho^\mathrm{Fe}\right)$ and ΔV_P refers to $\left(V_P^\mathrm{Core} - V_P^\mathrm{Fe}\right)$. We assume cross composition terms i.e., $\left(\frac{\mathrm{d}^2\rho}{\mathrm{d}C\mathrm{d}X_\mathrm{LE}}\right)$ and $\left(\frac{\mathrm{d}^2V_P}{\mathrm{d}C\mathrm{d}X_\mathrm{LE}}\right)$ are essentially negligible or "zero". This assumption has been successfully applied in prior studies[6,66,76]. We estimate the effect of light elements—O, S, Si, H, N on ρ and V_P of liquid iron i.e., $\left(\frac{\mathrm{d}\rho}{\mathrm{d}X_\mathrm{LE}}\right)$ and $\left(\frac{\mathrm{d}V_P}{\mathrm{d}X_\mathrm{LE}}\right)$ calculated from prior studies[6,59,62,65,66]. We estimate the effect of carbon on ρ and V_P of liquid iron i.e., $\left(\frac{\mathrm{d}\rho}{\mathrm{d}X_\mathrm{C}}\right)$ and $\left(\frac{\mathrm{d}V_P}{\mathrm{d}X_\mathrm{C}}\right)$ from this study (Fig. 3). In our analysis, we have not considered the effect of nickel but we do not anticipate a different result even if ~5–10 wt.% Ni is present in the outer core because previous FPMD studies showed that the effect of Ni on the ρ and V_P of liquid iron are small[6,65,66].

Our analysis shows that we are unable to simultaneously explain ρ and V_P for Earth's entire outer core by considering any Fe–C–LE ternary. However, we are able to explain ρ and V_P, simultaneously and provide a unique solution for C either at the CMB or the ICB conditions, with LE as O, S, and H but such solution is also not obtained if carbon is considered with Si, and N as light elements (Fig. 4). For the core adiabat with $T_\mathrm{CMB} =$ 6000 K, we are able to simultaneously explain ρ and V_P for Earth's outer core at CMB conditions with (a) ~2.7 wt.% C with ~3.1 wt.% O for a Fe–C–O ternary; (b) ~2.5 wt.% C with ~5.6 wt. % S for a Fe–C–S ternary; and (c) ~2.5 wt.% C with ~0.5 wt.% H for a Fe–C–H ternary. Similarly, we can simultaneously explain ρ and V_P for Earth's outer core along core adiabat of $T_\mathrm{ICB} = 6000$ K at ICB conditions with (a) ~0.3 wt.% C with ~6.2 wt.% O for a Fe–C–O ternary and (b) ~0 wt.% C with ~11.1 wt.% S for a Fe–C–S ternary. When the lower core adiabat with $T_\mathrm{ICB} = 5400$ K and 5000 K is considered, velocity and density can be explained with a lower concentration of carbon, which is compensated by a higher concentration of S and H. For example, with $T_\mathrm{CMB} = 3700$ K, ~1.6 wt.% carbon with ~9 wt.% S or ~0.8 wt.% H can simultaneously explain ρ and V_P at CMB. These analyses indicate that if carbon is a component in any model ternary outer core system, the closest solution is its concentration varying between 0 and 2.7 wt.% (Fig. 4). Our finding that the higher concentration of sulfur and hydrogen is favored at lower core temperatures is consistent with the large melting point depression of liquid Fe by S and H compared to that by C[40–42,45].

We find that carbon concentration between 0.3 and 2.7 wt.% can simultaneously explain ρ and V_P in the Earth's outer core when oxygen is considered as another light element. However, when we consider several light elements, LE = H, S, Si, and N in the Fe–C–LE ternary systems, our results show that the lower limit of carbon in the outer core could be as low as ~0 wt.%. However, parental alloy melt for magmatic iron meteorites can contain up to ~1100 ppm C[82–84]. Given iron meteorite parent bodies are the earliest formed protoplanets in the Solar System and have been argued to contribute volatile budget to later formed rocky embryos and planets[85], it is unlikely that the core of large terrestrial planets such as Earth would not sequester some carbon during the accretionary process. Combining the evidence from iron meteorites and our analysis from Fe–C–O ternary, we place the lower limit of carbon in the Earth's outer core to 0.3 wt. %. Additional constraints on the upper limit of carbon content by comparing the density contrast between the outer and inner core with the density difference between solid iron[86,87] and liquid Fe–C alloys from our study suggest that the outer core should not have any more than ~2 wt.% carbon (Supplementary Fig. S6)[29,30]. This is based on the assumption that carbon is the only a light element in the core and most of the carbon partitions into the liquid outer core. Our result on the ICB density discontinuity is consistent with recent constraints[28]. Thus, considering all of the above, we predict the expected range of carbon in the Earth's outer core to be as low as 0.3 wt.% and as high as 2.0 wt.%. Our predicted carbon concentration is consistent with the partitioning of carbon between silicate and metallic melts, which together with different accretional models and various assumptions of the extent of metal-silicate equilibration, provide a similar range of carbon content for the outer core ~0.1 wt.% to ~2 wt.%[12,20,23,27]. Our estimation is also similar to ~1.5–2.0 wt.% carbon proposed for the Earth's outer core by matching the density discontinuity at ICB[28]. Estimation based on the eutectic temperature in Fe–C phase diagram is less than 3 wt.%[33]. The outer core with >3 wt.% C could crystallize Fe_7C_3 phase at ICB[33], and their densities are too small to compensate for the inner-core density deficit[88]. If the higher end of the outer core C content as constrained by our study and that of earlier studies is applicable, then the effective partitioning of C to the core during metal-silicate separation is expected to be those predicted by most C partitioning studies that produced partition coefficients in the range of hundreds or higher[14,15,17].

Our study suggests that the Earth's outer core contains 0.3–2.0 wt.% C, i.e., $5.5 - 36.8 \times 10^{24}$ g of carbon, which is similar to some of the previous estimates[15,20,89]. There remains considerable uncertainty in the bulk Earth carbon budget, with recent estimates varying between ~220 and 1100 ppm[7,23,90]. Assuming the inner-core carbon concentration to be negligible based on the previous estimation of strong preference of C toward liquid outer core relative to solid inner core[28], and taking into account the recent estimates of the BSE carbon budget, i.e., 100–480 ppm[91,92], we can re-assess the bulk Earth carbon (BE) budget. Summing up the BSE and the core carbon budget, with the constraint for the latter from the present study, the BE carbon concentration could be as high as ~990–6460 ppm. Hence, the core could be the largest reservoir for carbon on Earth, accounting for as much as ~93–95% of the total terrestrial carbon. Therefore, if the upper limit of core C suggested by our study is relevant, Earth's carbon budget maybe distinctly larger than estimated in various recent studies that suggest carbon acted only as a mild siderophile element during core formation. Although our study places a non-zero lower bound of 0.3 wt.% for the outer core C, constraining a strict lower bound will require future investigations likely combining mineral physics, cosmochemistry, geochemistry, and dynamics of the formation of Earth-like rocky planets.

Methods

We used FPMD in canonical (*NVT*) ensemble as implemented in Vienna ab initio simulation package (VASP)[93–95]. The calculation of forces and energies is based on density functional theory (DFT) with projector-augmented wave (PAW) method[96]. We used the generalized gradient-approximation formulation (GGA-PBE)[97] which has been successfully used in the other metallic systems[25,58,59,98]. We used Γ-point sampling to integrate the Brillouin zone with the time step of 1 femtosecond, fs (where 1 fs = 10^{-15} s). We used a Nosé thermostat algorithm for constant temperature in our MD simulations[99]. We used an energy cutoff of 400 eV for the plane-wave basis set. To account the effect of limited cutoff energy, we added a volume-dependent Pulay correction (P_{Pulay}) to the pressure[100]. The P_{Pulay} increases with increasing pressure and for the explored pressure range, i.e., 0–360 GPa, P_{Pulay} varies from 0.5 to 1.5 GPa. To constrain the carbon content in the conditions relevant for the Earth's core, our calculations were performed in nonmagnetic liquid alloys. Previous experiments indicated that liquid Fe could exhibit magnetic moments at lower pressures of ~1 bar[101]. Recent FPMD simulation on liquid iron and iron alloys (Fe–Si–S) indicated that magnetic moments in liquid were sustained at higher pressures[102]. It is well known that in crystalline iron alloys, magnetism influences elastic properties. At low pressures, crystalline iron alloys are often magnetic, and they undergo pressure-induced loss of magnetism i.e., magnetic to nonmagnetic phase, and concomitant with that there is stiffening of elasticity including bulk modulus[103,104]. To test the effect of magnetic moment on energetics of iron (Fe) and iron-rich alloys (Fe–C), we performed FPMD calculations with magnetic moments at core conditions. We set a magnetic moment of

$\mu_m = 4\mu_B$ for each Fe atom in the liquid Fe and liquid Fe–C alloy. We found that the magnetic moments decrease to ~0 within 1 ps of simulation time. At core pressures and temperatures, the magnetic moments do not have any effect on the predicted pressure (Supplementary Fig. S7).

To explore how dissolved carbon affects the properties of liquid iron, we explored three different iron–carbon liquids, with a binary stoichiometry of $Fe_{66}C_{30}$ (~9 wt.% C), $Fe_{74}C_{22}$ (~6 wt.% C), and $Fe_{81}C_{15}$ (~4 wt.% C). A total of 96 atoms are simulated in a cubic box with periodic boundary conditions. We consider several constant volumes (densities) along four different isotherms (4000–7000 K). In addition to the high temperatures explored for assessing the properties at core conditions, we also simulated $Fe_{75}C_{21}$ (~5.7 wt.% carbon) at a temperature of ~2273 K. This is to assess the difference between the FPMD predicted pressures and the experimental pressures for the same melt density[47]. The densities explored in this study, corresponding to the pressure range of 0–360 GPa, i.e., covering the entire range of core pressures. For each fixed volume, we conducted the FPMD simulation at 7000 K for 10–20 ps (1 ps = 10^{-12} s). Temperature is then lowered to 6000 K within a shorter time of ~4 ps. We use these equilibrated cells and performed MD simulation for longer time scales ranging between 10 and 45 ps, and this procedure is repeated for lower isotherms of 5000 K and 4000 K. Similar procedure is implemented for all iron–carbon liquids. Examination of the radial distribution function (RDF) and mean square displacement (MSD) indicate the simulated structure is in a liquid state. RDF for each atomic pair exhibits a short to mid-range order and long-range disorder with a strong first peak followed by a minima and fluctuation of RDF close to unity at a larger distance (Supplementary Fig. S8). Log–log plot of MSD vs time shows a slope of unity and the MSD exceeded 10 $Å^2$ within our simulation time indicating that the melt exhibits ergodic behavior (Supplementary Fig. S9). We use the blocking method to determine the average energies and pressures for each simulation volume[105]. While taking an average, we discard the initial 10% of the data from the time series for the equilibration of the system. The time evolution of energy and pressure differences from the values averaged over the full simulation time shows that the results converge in a few picoseconds (ps) (Supplementary Fig. S9). Within ~4 ps of simulation time, the difference in pressure and energy decreases to ~0.5 GPa and ~0.01 eV per atom, respectively (Supplementary Fig. S9). We also explore the effect of pressure correction in calculated properties by considering a thermodynamically calculated empirical pressure correction (P^{th}_{corr}) (Supplementary Note S1 and Supplementary Figs. S2–S4).

Data availability

All the data used in this study are presented in the main paper and in the supplementary document. Parameters used in the simulation are described in the "Methods" section. Raw data used to produce Figs. 1–4 and Supplementary Figs. S1-S9 can be accessed from the public repository Zenodo: https://doi.org/10.5281/zenodo.4903530. The repository also contains the files with simulation input parameters as well as the positions files to compute the coordination statistics (Supplementary Fig. S1).

Code availability

Molecular dynamics simulations were performed using the Vienna ab initio simulation package (VASP) software which is available at https://www.vasp.at/.

Received: 23 December 2020; Accepted: 7 June 2021;
Published online: 19 August 2021

References

1. Birch, F. Elasticity and constitution of the Earth's interior. *J. Geophys. Res.* **57**, 227–286 (1952).
2. Birch, F. Density and composition of mantle and core. *J. Geophys. Res.* **69**, 4377–4388 (1964).
3. Anderson, O. & Isaak, D. Another look at the core density deficit of Earth's outer core. *Phys. Earth Planet. Inter.* **131**, 19–27 (2002).
4. Poirier, J.-P. Light elements in the Earth's outer core: a critical review. *Phys. Earth Planet. Inter.* **85**, 319–337 (1994).
5. Allègre, C. J., Poirier, J.-P., Humler, E. & Hofmann, A. W. The chemical composition of the Earth. *Earth Planet. Sci. Lett.* **134**, 515–526 (1995).
6. Badro, J., Côté, A. S. & Brodholt, J. P. A seismologically consistent compositional model of Earth's core. *Proc. Natl Acad. Sci. USA* **111**, 7542–7545 (2014).
7. McDonough, W. Compositional model for the Earth's core. *Treatise Geochem.* **2**, 547–568 (2003).
8. Wood, B. J. Carbon in the core. *Earth Planet. Sci. Lett.* **117**, 593–607 (1993).
9. Jeanloz, R. The nature of the Earth's core. *Annu. Rev. Earth Planet. Sci.* **18**, 357–386 (1990).
10. Li, J. & Fei, Y. Experimental constraints on core composition. *Treatise Geochem.* **3**, 493–519 (2003).
11. Nakajima, Y., Takahashi, E., Suzuki, T. & Funakoshi, K.-i. "Carbon in the core" revisited. *Phys. Earth Planet. Inter.* **174**, 202–211 (2009).
12. Dasgupta, R. & Walker, D. Carbon solubility in core melts in a shallow magma ocean environment and distribution of carbon between the Earth's core and the mantle. *Geochimica et Cosmochimica Acta* **72**, 4627–4641 (2008).
13. Chi, H., Dasgupta, R., Duncan, M. S. & Shimizu, N. Partitioning of carbon between Fe-rich alloy melt and silicate melt in a magma ocean–implications for the abundance and origin of volatiles in Earth, Mars, and the Moon. *Geochimica et Cosmochimica Acta* **139**, 447–471 (2014).
14. Dalou, C., Hirschmann, M. M., von der Handt, A., Mosenfelder, J. & Armstrong, L. S. Nitrogen and carbon fractionation during core–mantle differentiation at shallow depth. *Earth Planet. Sci. Lett.* **458**, 141–151 (2017).
15. Dasgupta, R., Chi, H., Shimizu, N., Buono, A. S. & Walker, D. Carbon solution and partitioning between metallic and silicate melts in a shallow magma ocean: implications for the origin and distribution of terrestrial carbon. *Geochimica et Cosmochimica Acta* **102**, 191–212 (2013).
16. Li, Y., Dasgupta, R. & Tsuno, K. The effects of sulfur, silicon, water, and oxygen fugacity on carbon solubility and partitioning in Fe-rich alloy and silicate melt systems at 3 GPa and 1600 °C: Implications for core–mantle differentiation and degassing of magma oceans and reduced planetary mantles. *Earth Planet. Sci. Lett.* **415**, 54–66 (2015).
17. Li, Y., Dasgupta, R., Tsuno, K., Monteleone, B. & Shimizu, N. Carbon and sulfur budget of the silicate Earth explained by accretion of differentiated planetary embryos. *Nat. Geosci.* **9**, 781–785 (2016).
18. Armstrong, L. S., Hirschmann, M. M., Stanley, B. D., Falksen, E. G. & Jacobsen, S. D. Speciation and solubility of reduced C–O–H–N volatiles in mafic melt: Implications for volcanism, atmospheric evolution, and deep volatile cycles in the terrestrial planets. *Geochimica et Cosmochimica Acta* **171**, 283–302 (2015).
19. Tsuno, K., Grewal, D. S. & Dasgupta, R. Core-mantle fractionation of carbon in Earth and Mars: the effects of sulfur. *Geochimica et Cosmochimica Acta* **238**, 477–495 (2018).
20. Dasgupta, R. & Grewal, D. S. Origin and early differentiation of carbon and associated life-essential volatile elements on Earth. in *Deep Carbon: Past to Present* (eds Orcutt, B. et al.) 4–39 (Cambridge University Press, 2019).
21. Malavergne, V. et al. Experimental constraints on the fate of H and C during planetary core-mantle differentiation. Implications for the Earth. *Icarus* **321**, 473–485 (2019).
22. Grewal, D. S. et al. The fate of nitrogen during core-mantle separation on Earth. *Geochimica et Cosmochimica Acta* **251**, 87–115 (2019).
23. Fischer, R. A., Cottrell, E., Hauri, E., Lee, K. K. & Le Voyer, M. The carbon content of Earth and its core. *Proc. Natl Acad. Sci. USA* **117**, 8743–8749 (2020).
24. Fichtner, C. E., Schmidt, M. W., Liebske, C., Bouvier, A.-S. & Baumgartner, L. P. Carbon partitioning between metal and silicate melts during Earth accretion. *Earth Planet. Sci. Lett.* **554**, 116659 (2021).
25. Zhang, Y. & Yin, Q.-Z. Carbon and other light element contents in the Earth's core based on first-principles molecular dynamics. *Proc. Natl Acad. Sci. USA* **109**, 19579–19583 (2012).
26. Solomatova, N. V., Caracas, R. & Manning, C. E. Carbon sequestration during core formation implied by complex carbon polymerization. *Nat. Commun.* **10**, 789 (2019).
27. Wood, B. J., Li, J. & Shahar, A. Carbon in the core: its influence on the properties of core and mantle. *Rev. Mineral. Geochem.* **75**, 231–250 (2013).
28. Li, Y., Vočadlo, L., Alfè, D. & Brodholt, J. Carbon partitioning between the Earth's inner and outer core. *J. Geophys. Res.: Solid Earth* **124**, 12812–12824 (2019).
29. Tkalčić, H., Kennett, B. L. & Cormier, V. F. On the inner—outer core density contrast from PKiKP/PcP amplitude ratios and uncertainties caused by seismic noise. *Geophys. J. Int.* **179**, 425–443 (2009).
30. Masters, G. & Gubbins, D. On the resolution of density within the Earth. *Physics Earth Planet. Inter.* **140**, 159–167 (2003).
31. Lord, O., Walter, M., Dasgupta, R., Walker, D. & Clark, S. Melting in the Fe–C system to 70 GPa. *Earth Planet. Sci. Lett.* **284**, 157–167 (2009).
32. Morard, G. et al. Fe–FeO and Fe–Fe_3C melting relations at Earth's core–mantle boundary conditions: implications for a volatile-rich or oxygen-rich core. *Earth Planet. Sci. Lett.* **473**, 94–103 (2017).
33. Mashino, I., Miozzi, F., Hirose, K., Morard, G. & Sinmyo, R. Melting experiments on the Fe–C binary system up to 255 GPa: constraints on the carbon content in the Earth's core. *Earth Planet. Sci. Lett.* **515**, 135–144 (2019).
34. Chen, B. et al. Experimental constraints on the sound velocities of cementite Fe_3C to core pressures. *Earth Planet. Sci. Lett.* **494**, 164–171 (2018).
35. Prescher, C. et al. High Poisson's ratio of Earth's inner core explained by carbon alloying. *Nat. Geosci.* **8**, 220–223 (2015).
36. Mookherjee, M. et al. High-pressure behavior of iron carbide (Fe_7C_3) at inner core conditions. *J. Geophys. Res.* **116**, B04201 (2011).
37. Hirose, K. et al. Hydrogen limits carbon in liquid iron. *Geophys. Res. Lett.* **46**, 5190–5197 (2019).

38. Sinmyo, R., Hirose, K. & Ohishi, Y. Melting curve of iron to 290 GPa determined in a resistance-heated diamond-anvil cell. *Earth Planet. Sci. Lett.* **510**, 45–52 (2019).
39. Anzellini, S., Dewaele, A., Mezouar, M., Loubeyre, P. & Morard, G. Melting of iron at Earth's inner core boundary based on fast X-ray diffraction. *Science* **340**, 464–466 (2013).
40. Fischer, R. A. Melting of Fe-alloys and the thermal structure of the core. *Deep Earth: Phys. Chem. Lower Mantle Core* **217**, 3–12 (2016).
41. Mori, Y. et al. Melting experiments on Fe–Fe_3S system to 254 GPa. *Earth Planet. Sci. Lett.* **464**, 135–141 (2017).
42. Shibazaki, Y. et al. High-pressure and high-temperature phase diagram for $Fe_{0.9}Ni_{0.1}$–H alloy. *Phys. Earth Planet. Inter.* **228**, 192–201 (2014).
43. Seagle, C., Heinz, D., Campbell, A., Prakapenka, V. & Wanless, S. Melting and thermal expansion in the Fe–FeO system at high pressure. *Earth Planet. Sci. Lett.* **265**, 655–665 (2008).
44. Fischer, R. A. et al. Phase relations in the Fe–FeSi system at high pressures and temperatures. *Earth Planet. Sci. Lett.* **373**, 54–64 (2013).
45. Fei, Y. & Brosh, E. Experimental study and thermodynamic calculations of phase relations in the Fe–C system at high pressure. *Earth Planet. Sci. Lett.* **408**, 155–162 (2014).
46. Jimbo, I. & Cramb, A. The density of liquid iron-carbon alloys. *Metallurg. Transac. B* **24**, 5–10 (1993).
47. Sanloup, C., Van Westrenen, W., Dasgupta, R., Maynard-Casely, H. & Perrillat, J.-P. Compressibility change in iron-rich melt and implications for core formation models. *Earth Planet. Sci. Lett.* **306**, 118–122 (2011).
48. Shimoyama, Y. et al. Density of Fe-3.5 wt% C liquid at high pressure and temperature and the effect of carbon on the density of the molten iron. *Phys. Earth Planet. Inter.* **224**, 77–82 (2013).
49. Shimoyama, Y. et al. Thermoelastic properties of liquid Fe-C revealed by sound velocity and density measurements at high pressure. *J. Geophys. Res.: Solid Earth* **121**, 7984–7995 (2016).
50. Terasaki, H. et al. Density measurement of Fe_3C liquid using X-ray absorption image up to 10 GPa and effect of light elements on compressibility of liquid iron. *J. Geophys. Res.: Solid Earth* **115**, B06207 (2010).
51. Kuwabara, S. et al. Sound velocity and elastic properties of Fe–Ni and Fe–Ni–C liquids at high pressure. *Phys. Chem. Minerals* **43**, 229–236 (2016).
52. Morard, G. et al. Structure and density of Fe-C liquid alloys under high pressure. *J. Geophys. Res.: Solid Earth* **122**, 7813–7823 (2017).
53. Nakajima, Y. et al. Carbon-depleted outer core revealed by sound velocity measurements of liquid iron-carbon alloy. *Nat. Commun.* **6**, 1–7 (2015).
54. Birch, F. The velocity of compressional waves in rocks to 10 kilobars: 2. *J. Geophys. Res.* **66**, 2199–2224 (1961).
55. Badro, J. et al. Effect of light elements on the sound velocities in solid iron: Implications for the composition of Earth's core. *Earth Planet. Sci. Lett.* **254**, 233–238 (2007).
56. Lin, J.-F. et al. Sound velocities of hot dense iron: Birch's law revisited. *Science* **308**, 1892–1894 (2005).
57. Umemoto, K. et al. Liquid iron-sulfur alloys at outer core conditions by first-principles calculations. *Geophys. Res. Lett.* **41**, 6712–6717 (2014).
58. Ichikawa, H., Tsuchiya, T. & Tange, Y. The P-V-T equation of state and thermodynamic properties of liquid iron. *J. Geophys. Res.: Solid Earth* **119**, 240–252 (2014).
59. Bajgain, S. K., Mookherjee, M., Dasgupta, R., Ghosh, D. B. & Karki, B. B. Nitrogen content in the Earth's outer core. *Geophys. Res. Lett.* **46**, 89–98 (2019).
60. Huang, D., Badro, J., Brodholt, J. & Li, Y. Ab initio molecular dynamics investigation of molten Fe-Si-O in Earth's core. *Geophys. Res. Lett.* **46**, 6397–6405 (2019).
61. Umemoto, K. & Hirose, K. Liquid iron-hydrogen alloys at outer core conditions by first-principles calculations. *Geophys. Res. Lett.* **42**, 7513–7520 (2015).
62. Fu, J., Cao, L., Duan, X. & Belonoshko, A. B. Density and sound velocity of liquid Fe-S alloys at Earth's outer core P-T conditions. *Am. Mineralogist* **105**, 1349–1354 (2020).
63. Lai, X., Chen, B., Wang, J., Kono, Y. & Zhu, F. Polyamorphic transformations in Fe-Ni-C liquids: implications for chemical evolution of terrestrial planets. *J. Geophys. Res.: Solid Earth* **122**, 9745–9754 (2017).
64. Wang, J., Chen, B., Williams, Q. & Manghnani, M. Short-and intermediate-range structure and dynamics of Fe-Ni-C liquid under compression. *Front. Earth Sci.* **7**, 258 (2019).
65. Ichikawa, H. & Tsuchiya, T. Ab Initio thermoelasticity of liquid iron-nickel-light element alloys. *Minerals* **10**, 59 (2020).
66. Umemoto, K. & Hirose, K. Chemical compositions of the outer core examined by first principles calculations. *Earth Planet. Sci. Lett.* **531**, 116009 (2020).
67. French, M. & Mattsson, T. R. Thermodynamically constrained correction to ab initio equations of state. *J. Appl. Phys.* **116**, 013510 (2014).
68. Wagle, F. & Steinle-Neumann, G. Liquid iron equation of state to the terapascal regime from ab initio simulations. *J. Geophys. Res.: Solid Earth* **124**, 3350–3364 (2019).
69. Alfè, D., Price, G. & Gillan, M. Iron under Earth's core conditions: liquid-state thermodynamics and high-pressure melting curve from ab initio calculations. *Phys. Rev. B* **65**, 165118 (2002).
70. Rivers, M. L. & Carmichael, I. S. Ultrasonic studies of silicate melts. *J. Geophys. Res.: Solid Earth* **92**, 9247–9270 (1987).
71. Dziewonski, A. M. & Anderson, D. L. Preliminary reference Earth model. *Phys. Earth Planet. Inter.* **25**, 297–356 (1981).
72. Alfè, D. Temperature of the inner-core boundary of the Earth: melting of iron at high pressure from first-principles coexistence simulations. *Phys. Rev. B* **79**, 1–5 (2009).
73. Vočadlo, L., Alfe, D., Gillan, M. & Price, G. D. The properties of iron under core conditions from first principles calculations. *Phys. Earth Planet. Inter.* **140**, 101–125 (2003).
74. Antonangeli, D. et al. Simultaneous sound velocity and density measurements of hcp iron up to 93 GPa and 1100 K: An experimental test of the Birch's law at high temperature. *Earth Planet. Sci. Lett.* **331**, 210–214 (2012).
75. Sakaiya, T. et al. Sound velocity and density measurements of liquid iron up to 800 GPa: a universal relation between Birch's law coefficients for solid and liquid metals. *Earth Planet. Sci. Letters* **392**, 80–85 (2014).
76. Huang, H. et al. Evidence for an oxygen-depleted liquid outer core of the Earth. *Nature* **479**, 513–516 (2011).
77. Siebert, J., Badro, J., Antonangeli, D. & Ryerson, F. J. Terrestrial accretion under oxidizing conditions. *Science* **339**, 1194–1197 (2013).
78. Fischer, R. A. et al. High pressure metal–silicate partitioning of Ni, Co, V, Cr, Si, and O. *Geochimica et Cosmochimica Acta* **167**, 177–194 (2015).
79. Helffrich, G. & Kaneshima, S. Seismological constraints on core composition from Fe-O-S liquid immiscibility. *Science* **306**, 2239–2242 (2004).
80. Badro, J., Brodholt, J. P., Piet, H., Siebert, J. & Ryerson, F. J. Core formation and core composition from coupled geochemical and geophysical constraints. *Proc. Natl Acad. Sci. USA* **112**, 12310–12314 (2015).
81. Alfe, D., Gillan, M. & Price, G. Composition and temperature of the Earth's core constrained by combining ab initio calculations and seismic data. *Earth Planet. Sci. Lett.* **195**, 91–98 (2002).
82. Sugiura, N. Ion probe measurements of carbon and nitrogen in iron meteorites. *Meteoritics Planet. Sci.* **33**, 393–409 (1998).
83. Goldstein, J. I., Huss, G. R. & Scott, E. R. Ion microprobe analyses of carbon in Fe–Ni metal in iron meteorites and mesosiderites. *Geochimica et Cosmochimica Acta* **200**, 367–407 (2017).
84. Hirschmann, M. M., Bergin, E. A., Blake, G. A., Ciesla, F. J. & Li, J. Early volatile depletion on planetesimals inferred from C–S systematics of iron meteorite parent bodies. *Proc. Natl Acad. Sci. USA* **118**, 1–8 (2021).
85. Grewal, D. S., Dasgupta, R. & Marty, B. A very early origin of isotopically distinct nitrogen in inner solar system protoplanets. *Nat. Astronomy* **5**, 356–364 (2021).
86. Dewaele, A. et al. Quasihydrostatic equation of state of iron above 2 Mbar. *Phys. Rev. Lett.* **97**, 215504 (2006).
87. Miozzi, F. et al. A new reference for the thermal equation of state of iron. *Minerals* **10**, 100 (2020).
88. Li, Y., Vočadlo, L., Brodholt, J. & Wood, I. Thermoelasticity of Fe_7C_3 under inner core conditions. *J. Geophys. Res.: Solid Earth* **121**, 5828–5837 (2016).
89. Dasgupta, R. & Hirschmann, M. M. The deep carbon cycle and melting in Earth's interior. *Earth Planet. Sci. Lett.* **298**, 1–13 (2010).
90. Marty, B. The origins and concentrations of water, carbon, nitrogen and noble gases on Earth. *Earth Planet. Sci. Lett.* **313**, 56–66 (2012).
91. Marty, B. et al. An evaluation of the C/N ratio of the mantle from natural CO_2-rich gas analysis: geochemical and cosmochemical implications. *Earth Planet. Sci. Lett.* **551**, 116574 (2020).
92. Hirschmann, M. M. Comparative deep Earth volatile cycles: the case for C recycling from exosphere/mantle fractionation of major (H_2O, C, N) volatiles and from H_2O/Ce, CO_2/Ba, and CO_2/Nb exosphere ratios. *Earth Planet. Sci. Lett.* **502**, 262–273 (2018).
93. Kresse, G. & Hafner, J. Ab initio molecular dynamics for liquid metals. *Phys. Rev. B* **47**, 558–561 (1993).
94. Kresse, G. & Furthmüller, J. Efficiency of ab-initio total energy calculations for metals and semiconductors using a plane-wave basis set. *Computat. Mater. Sci.* **6**, 15–50 (1996).
95. Kresse, G. & Furthmüller, J. Efficient iterative schemes for ab initio total-energy calculations using a plane-wave basis set. *Phys. Rev. B* **54**, 11169–11186 (1996).
96. Kresse, G. & Joubert, D. From ultrasoft pseudopotentials to the projector augmented-wave method. *Phys. Rev. B* **59**, 1758 (1999).
97. Perdew, J. P., Burke, K. & Ernzerhof, M. Generalized gradient approximation made simple. *Phys. Rev. Lett.* **77**, 3865–3868 (1996).
98. Pozzo, M., Davies, C., Gubbins, D. & Alfè, D. Transport properties for liquid silicon-oxygen-iron mixtures at Earth's core conditions. *Phys. Rev. B* **87**, 014110 (2013).
99. Nosé, S. A unified formulation of the constant temperature molecular dynamics methods. *J. Chem. Phys.* **81**, 511–519 (1984).

100. Francis, G. & Payne, M. Finite basis set corrections to total energy pseudopotential calculations. *J. Phys.: Condensed Matter* **2**, 4395–4404 (1990).
101. Waseda, Y. & Suzuki, K. Atomic distribution and magnetic moment in liquid iron by neutron diffraction. *Physics Status Solidi* **B39**, 669–678 (1970).
102. Edgington, A. et al. The top-down crystallisation of Mercury's core. *Earth Planet. Sci. Lett.* **528**, 115838 (2019).
103. Vočadlo, L. et al. The effect of ferromagnetism on the equation of state of Fe_3C studied by first-principles calculations. *Earth Planet. Sci. Lett.* **203**, 567–575 (2002).
104. Mookherjee, M. Elasticity and anisotropy of Fe_3C at high pressures. *Am. Mineralogist* **96**, 1530–1536 (2011).
105. Flyvbjerg, H. & Petersen, H. G. Error estimates on averages of correlated data. *J. Chem. Phys.* **91**, 461–466 (1989).
106. Anderson, W. W. & Ahrens, T. J. An equation of state for liquid iron and implications for the Earth's core. *J. Geophys. Res.: Solid Earth* **99**, 4273–4284 (1994).
107. Brown, J. M. & McQueen, R. G. Phase transitions, Grüneisen parameter, and elasticity for shocked iron between 77 GPa and 400 GPa. *J. Geophys. Res.: Solid Earth* **91**, 7485–7494 (1986).
108. Kuwayama, Y. et al. Equation of state of liquid iron under extreme conditions. *Phys. Rev. Lett.* **124**, 165701 (2020).

Acknowledgements

Authors would like to thank three anonymous reviewers for their insightful comments that helped improve the clarity of the article. M.M. and S.B. acknowledge the National Science Foundation grants (EAR1763215 and EAR1753125) for funding this research and thank the Extreme Science and Engineering Discovery (XSEDE) supercomputing facilities (TG-GEO170003) and the Research Computing Center (RCC) at Florida State University (FSU) for computing resources. R.D. acknowledges NASA grants 80NSSC18K0828 and 80NSSC18K1314.

Author contributions

S.B., M.M., and R.D. conceived the project. S.B. performed the simulations. All three authors contributed to the analysis, discussion, and writing of the article.

Competing interests

The authors declare no competing interests.

Additional information

Supplementary information The online version contains supplementary material available at https://doi.org/10.1038/s43247-021-00222-7.

Correspondence and requests for materials should be addressed to S.K.B.

Peer review information *Communications Earth & Environment* thanks the anonymous reviewers for their contribution to the peer review of this work. Primary Handling Editor: Joe Aslin. Peer reviewer reports are available.

Reprints and permission information is available at http://www.nature.com/reprints

Publisher's note Springer Nature remains neutral with regard to jurisdictional claims in published maps and institutional affiliations.